Vehicle Sideslip Estimator using Load Sensing Bearings

Anil Kunnappillil Madhusudhanan[a,b], Matteo Corno[c], Edward Holweg[a,d]

[a]*Intelligent Automotive Systems Group, Precision and Microsystems Engineering Department, Delft University of Technology, Mekelweg 2, 2628 CD Delft, The Netherlands, email: a.k.madhu@tudelft.nl.*
[b]*Integrated Vehicle Safety Department, The Netherlands Organisation for Applied Scientific Research (TNO), Automotive Campus 30, 5708 JZ Helmond, The Netherlands, email: anil.madhu@tno.nl*
[c]*Dipartimento di Elettronica, Informazione e Bioingegneria, Politecnico di Milano, Via Ponzio 34/5, 20133 Milano, Italy.*
[d]*SKF Automotive Division, Nieuwegein 3430 DT, The Netherlands.*

Abstract

This paper investigates the potential of load based vehicle sideslip estimation. Different techniques to measure tyre forces have been presented over the years; so far no technique has made it to the market. This paper considers a new technology based on load sensing bearings, an industrially viable technology, which provides accurate tyre force measurements. Based on the features of the sensor, a vehicle sideslip angle estimator is designed, analyzed and tested. The paper shows that direct tyre force sensing has mainly two advantages over traditional model-based estimators: primarily, it avoids the use of tyre models, which are heavily affected by uncertainties and modeling errors and secondarily, providing measurements on the road plane, it is less prone to errors introduced by roll and pitch dynamics. Extensive simulation tests along with a detailed analysis of experimental tests performed on an instrumented vehicle prove that the load based estimation outperforms the kinematic model-based benchmark yielding a root mean square error of 0.15°.

Keywords: Vehicle sideslip, Kalman filter, state estimation, observability, Load Sensing Bearing

1. Introduction

The field of wheeled vehicle active dynamics control is extremely active and vibrant both from the academy and industrial point of views. Active safety systems, of which Electronic Stability Control (ESC) [1], Electronic Brake Distribution (EBD) [43] and torque vectoring [42] are examples, improve vehicle stability during critical maneuvers by applying feedback control using braking, drive or steering actuators. Many vehicle dynamics control (VDC) systems (see for example [1, 3, 4]) need to monitor, if not control in closed loop, the vehicle sideslip angle. The vehicle sideslip angle, defined as the angle between the vehicle longitudinal axis and the vehicle velocity vector, affects many dynamic properties of the vehicle. It determines, for example, the vehicle yaw moment sensitivity to steering angle [5, 6, 7]. This characteristic makes the vehicle yaw moment less sensitive to steering at higher vehicle sideslip. Furthermore, for certain range of vehicle sideslip and its time derivative, the vehicle motion is stable whereas outside this range *i.e.* outside this stability area, the vehicle yaw dynamics are unstable. In addition, as the steering angle increases, the stability area shrinks [8].

For the above reasons, the design and study of vehicle sideslip estimation methods has grown into a specific subfield of the VDC literature. Many estimation methods have been presented.

They can be classified along two main axes. On the one hand, different sensor suites call for different approaches; on the other hand, even within a given sensor configuration, different modeling approaches are possible.

Based on the type of sensors, the estimators can be classified into three main categories; using only inertial measurement sensors, using inertial measurement sensors and GPS, and using more exotic sensors. Thanks to the progress of MEMS technology, nowadays the basic vehicle sensor configuration is represented by three accelerometers, three gyros, four wheel encoders and steering angle. As the cost and availability of GPS sensors continues to decrease, the integration of the GPS to this basic vehicle configuration has been considered [9, 44, 45]. The GPS information increases the estimator accuracy; however GPS signals are known not to be reliable in some conditions, for example, buildings in urban environment can degrade GPS accuracy. In the third category, other sensors have been considered. For example, [47] considers magnetometers (with the obvious risk of disturbance and noise), or [48] uses steering torque measurements to improve the sideslip estimation. In [54], a sideslip estimator is proposed using lateral tyre force sensors and a linear tyre model. The estimator is computationally inexpensive and effective for lateral accelerations under 0.6 g on a dry road. However, the estimator performance is not studied for lateral accelerations in the range $[0.6, 1]$ g where the tyre characteristics becomes nonlinear and the need for accurate sideslip estimators is more pressing. In addition, longitudinal tyre slips are assumed to be negligible and this might degrade the estimator performance during combined tyre slip situations.

Contributions can also be classified based on the estimation methods; all estimation approaches are model-based. Based on the type of model employed, one can distinguish dynamic model-based method, and kinematic model-based methods.

At the core of kinematic model-based methods lie the kinematic relations between velocities, accelerations and angular rates. These methods neglect the forces that act on the vehicle. The kinematic model has the advantage of not depending on any physical parameter and as a consequence model calibration is simple and not affected by uncertainties. A well known nonlinear vehicle state observer was first introduced in [18] and proved to be asymptotically stable for all cornering conditions (non-zero yaw rate). The method is later strengthen by an online sensor bias estimation in [37, 19]. A similar method, with a more advance Extended Kalman Filter (EKF), is presented in [49]. The authors experimentally demonstrate the effectiveness of the method on short maneuvers. [50] develops a sliding mode observer based on the kinematic model; the observer is tested and analyzed in simulation. Kinematic model-based methods are reliable during transient maneuvers, and are robust to variation of the tyre characteristics, but suffer from estimation errors on nearly steady-state conditions. This issue is caused by an intrinsic lack of observability of the model when the yaw rate is close to zero.

Dynamic model-based methods can overcome the observability limitation. These approaches are based on dynamical models *i.e* models that describe the tyre force generation mechanism and how it affects the vehicle dynamics. These models have the potential of being very accurate, but require a tyre model. Many tyre models are available in the literature and are characterized by different level of complexity and accuracy. The simplest model introduces the concept of cornering stiffness, which is a linearization of the tyre force characteristics. The most used one is probably the semi-empirical Pacejka Model [12]; other approaches are presented in [13, 14]. These models, when calibrated on very specific conditions are very accurate; however the tyre forces depend on many factors that are not generally known a priori: road friction, tyre pressure and temperature to name a few. Identifying these parameters online has proven to be extremely challenging. Nevertheless

dynamic-based models are used in a number of contributions. In [15], an extended Kalman filter using adaptive linear tyre force model is studied. The tyre saturation characteristic is not considered in this work; for the method to work, the lateral tyre forces should be more than 2000 N. The estimator proposed in [16] is interesting as it uses online tyre cornering stiffness estimation. However it does not work on low friction surfaces such as ice and snow. In [17], a nonlinear observer is designed to estimate vehicle sideslip by solving Linear Matrix Inequalities (LMIs) and the estimator gives accurate results. However, solving LMIs real-time is computationally expensive. In [10] four types of sideslip estimators are designed and compared: a linear observer, a nonlinear observer, an extended Kalman filter and a sliding-mode observer. From this insightful comparison, the best among the four, the sliding-mode observer, is studied using a test vehicle in [11] showing good results for lateral accelerations lower than 0.6 g. Dynamic model-based methods do not suffer from observability limitations, but they suffer from limitation due to the unknown nonlinear characteristic of the tires.

In general, dynamic and kinematic based methods have complementary properties: kinematic methods are accurate for large sideslip angles; dynamic methods are more dependable for low sideslip angles, where the kinematic model losses observability. In [20, 51, 52], this complementarity is at the basis of the idea of integrating both approaches. At low frequencies, the physical model-based estimator is used and at high frequencies, the kinematic model-based estimator is used. This appropach requires delicate fusion or blending methods.

The estimator proposed in this paper fuses the positive features of the kinematic and dynamic approaches by using a novel sensor configuration. The proposed sideslip estimator employs a new Load Sensing Bearing (LSB) technology which can provide tyre force measurements [33]. Researches have been working on reliable and industrially viable methods to measure tyre force for years. Now, several sensor configurations are becoming available. Car manufacturers have been using measurement wheels (see for example Corrsys product [34]) to test their vehicles for years; other options include LSB from SKF [21], tyre-embedded force sensor [22], lateral tyre force sensor from NSK [23, 24, 25] and wheel force transducer [26]. The force sensor proposed in [22] embeds the sensor inside the tyre; this yields one measurement per revolution and a sensor that is subject to tear and wear. In [23, 24, 25], the lateral tyre force sensor from NSK is used to control vehicle motion. However, for sideslip estimation, the longitudinal tyre forces are also required, especially during combined tyre slip situations. The embedded force sensor in [22] and the wheel force transducer in [26] require wireless transmission of the measurements. Among the above approaches, bearing based technology is of particular interest because bearings are not subject to wear as tires, but are spatially close to the contact patch and can thus yield accurate measurement. Furthermore, the bearing being stationary, wireless data transfer is not necessary. Tyre force sensing is a realistic possibility in the near future and its advantages in terms of VDC warrants investigation. Tyre force-based control has been proven successful in lateral and longitudinal vehicle dynamics control [21, 27, 28, 29, 30]. The present work is an extension of [31] and studies the tyre force based vehicle sideslip estimation as it is important to implement and test the lateral vehicle dynamics control proposed in [29, 30]. The main contributions of this work are:

1. The characteristics of the LSB sensors are studied in details and compared against the Corrsys measurement wheels.
2. Based on the sensor characteristics, a LSB based sideslip Kalman filter is proposed. The proposed vehicle sideslip is based on a model relating vehicle velocities and forces in the longitudinal and lateral directions, and yaw rate. The analysis shows that the observer is

robust to tyre nonlinearities and roll and pitch unmodelled dynamics.

3. The estimator is validated using real-life experimental data from a test vehicle.
4. A heuristic method to overcome the estimate drift, caused by the unobservability when the vehicle yaw rate is close to zero, is proposed. The effects in terms of accuracy are studied in simulation as well as experimental results.
5. The estimator is studied for robustness against measurement noise and different road frictions.

A multibody vehicle model with 15 mechanical degrees of freedom (DOF) from CarSim simulation package [32] is used to evaluate the proposed estimator. CarSim model uses a nonlinear tyre model with dependency on slip, load, and camber. See the vehicle configuration *Ind_Ind: B-Class, Hatchback: No ABS* in CarSim for more details about the vehicle model. The test data used to validate the estimator is obtained with a BMW 5 Series E60 model equipped with LSB technology.

The paper is structured as follows. In Section 2, the kinematic model is discussed. Section 3 provides a detailed analysis on the LSB technology. The Kalman filter design is presented in Section 4 and the estimator used to compare the proposed estimator is introduced in Section 5. Section 6 shows validation of the proposed method in simulation using CarSim and also using real-life experimental data from the test vehicle. Finally, Section 7 concludes the work.

2. Kinematic Model

The model used to design the vehicle sideslip estimator is explained in this section. The planar kinematic model of the vehicle is given in (1):

$$\begin{bmatrix} \dot{v}_x \\ \dot{v}_y \end{bmatrix} = \begin{bmatrix} 0 & \dot{\psi} \\ -\dot{\psi} & 0 \end{bmatrix} \begin{bmatrix} v_x \\ v_y \end{bmatrix} + \begin{bmatrix} a_x \\ a_y \end{bmatrix}, \tag{1}$$

where $\dot{\psi}$ is the planar yaw rate, v_x and v_y are the vehicle longitudinal and lateral velocities, and a_x and a_y are the planar longitudinal and lateral accelerations of the center of gravity. Accelerations are measured through MEMS accelerometers and when vehicle is subject to pitches or roll, the measurements are corrupted by the gravitational acceleration [35, 40]. Accounting for this phenomenon transforms (1) into:

$$\begin{bmatrix} \dot{v}_x \\ \dot{v}_y \end{bmatrix} = \begin{bmatrix} 0 & \dot{\psi}_m \cos\theta \cos\phi \\ -\dot{\psi}_m \cos\theta \cos\phi & 0 \end{bmatrix} \begin{bmatrix} v_x \\ v_y \end{bmatrix} + \begin{bmatrix} (a_{x,m} + g\sin\theta)/\cos\theta \\ (a_{y,m} - g\cos\theta\sin\phi)/\cos\phi \end{bmatrix}, \tag{2}$$

where $\dot{\psi}_m$ is the measured yaw rate, $a_{x,m}$ and $a_{y,m}$ are the measured accelerations, θ is the pitch angle, ϕ is the roll angle and g is the gravity acceleration. The correction terms are added in (2) to translate the measured yaw rate $\dot{\psi}_m$ into the planar yaw rate $\dot{\psi}$, and the measured accelerations $a_{x,m}$ and $a_{y,m}$ into the planar accelerations a_x and a_y. In (2), the yaw rate measurements are distorted by a cosine term whereas the gravity acceleration enters with a sine term on the accelerations. Therefore, the acceleration measurement errors are more influential. These gravitational terms, if not compensated, negatively affect the accuracy of any acceleration based estimation. On the other hand, if tyre force measurements are used, the roll and pitch dynamics do not affect the estimation model as the tyre force measurements represent the forces acting at the tyre-road contact patches, thus on the plane of interest. In this work, such an approach is taken. The differential equations in (3) represent the model used to design the sideslip estimator proposed in this paper.

$$\begin{bmatrix} \dot{v}_x \\ \dot{v}_y \end{bmatrix} = \begin{bmatrix} 0 & \dot{\psi} \\ -\dot{\psi} & 0 \end{bmatrix} \begin{bmatrix} v_x \\ v_y \end{bmatrix} + \begin{bmatrix} \frac{1}{m} & 0 \\ 0 & \frac{1}{m} \end{bmatrix} \begin{bmatrix} F_x \\ F_y \end{bmatrix}. \tag{3}$$

In (3), m is the vehicle mass, and F_x and F_y are the vehicle planar longitudinal and lateral forces. The planar longitudinal and lateral forces F_x and F_y are related to the measured tyre forces as described by (**??**) and (**??**).

$$\begin{aligned} F_x &= F_{x_{FL}} - F_{y_{FL}}\delta_{FL} + F_{x_{FR}} - F_{y_{FR}}\delta_{FR} + F_{x_{RL}} - F_{y_{RL}}\delta_{RL} + F_{x_{RR}} - F_{y_{RR}}\delta_{RR} - C_{aer}A_L\frac{\rho}{2}v_x^2 \\ F_y &= F_{y_{FL}} + F_{x_{FL}}\delta_{FL} + F_{y_{FR}} + F_{x_{FR}}\delta_{FR} + F_{y_{RL}} + F_{x_{RL}}\delta_{RL} + F_{y_{RR}} + F_{x_{RR}}\delta_{RR}, \end{aligned} \tag{4}$$

where $F_{x_{ij}}$ and $F_{y_{ij}}$ are the longitudinal and lateral forces of ij tyre, C_{aer} is the coefficient of aerodynamic drag, A_L is the front vehicle area, ρ is the air density and δ_{ij} is the road steering angle of ij tyre. In (4), small angle approximations $\sin\delta \approx \delta$ and $\cos\delta \approx 1$ are used. As shown in (5) and (6), the model in (3) is now written in its state space representation:

$$\dot{x} = A(t)x + B(t)u + w, \tag{5}$$

$$y = Cx + v. \tag{6}$$

Here $A(t) = \begin{bmatrix} 0 & \dot{\psi} \\ -\dot{\psi} & 0 \end{bmatrix}$, $x = \begin{bmatrix} v_x \\ v_y \end{bmatrix}$, $B(t) = \begin{bmatrix} \frac{1}{m} & 0 \\ 0 & \frac{1}{m} \end{bmatrix}$, $u = \begin{bmatrix} F_x \\ F_y \end{bmatrix}$, w is the process noise, $y = v_x$, $C = \begin{bmatrix} 1 & 0 \end{bmatrix}$ and v is the measurement noise. The longitudinal velocity v_x measurement or estimate is assumed to be available. It can be estimated using a weighted average of the four wheel measurements, as usually done in ABS systems [36]. The yaw rate $\dot{\psi}$ and tyre forces are measured, and the lateral velocity v_y is the state to be estimated.

The vehicle sideslip β is shown graphically in Figure 1 as the angle between the vehicle longitudinal axis and the vehicle velocity vector. It is defined mathematically by (7):

$$\beta \approx \frac{v_y}{v_x}. \tag{7}$$

To get an estimate of the vehicle sideslip β, the lateral velocity v_y state in (5) needs to be estimated. This is further discussed in Section 4.

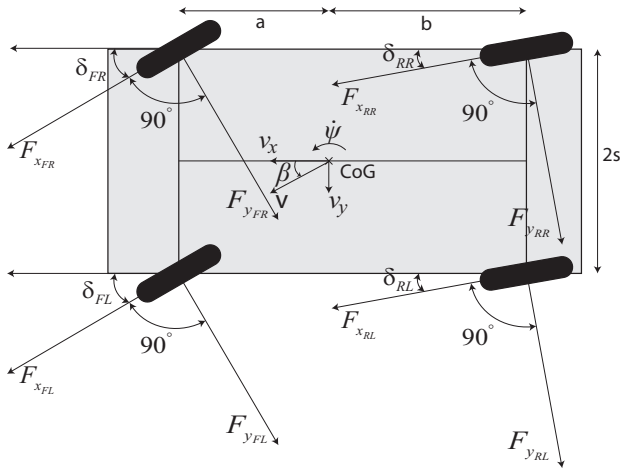

Figure 1: Two-track vehicle model.

3. Load Sensing Bearing

Currently, the state-of-the-art tyre force sensing is represented by measurement wheels. These systems are accurate, but are not viable for commercial use because of high cost, encumbrance and complex calibration procedures. In the past few years, several solutions to provide more cost-effective tyre force sensing have been proposed [22, 23, 24, 25, 26]. Although none of them is currently at production level, cost effective tyre force sensing is expected to become a reality. LSB technology from SKF [33] is one of the most interesting solutions because it measures tyre forces in addition to their primary objective of acting as a bearing. Figure 2(b) shows a LSB unit from SKF.

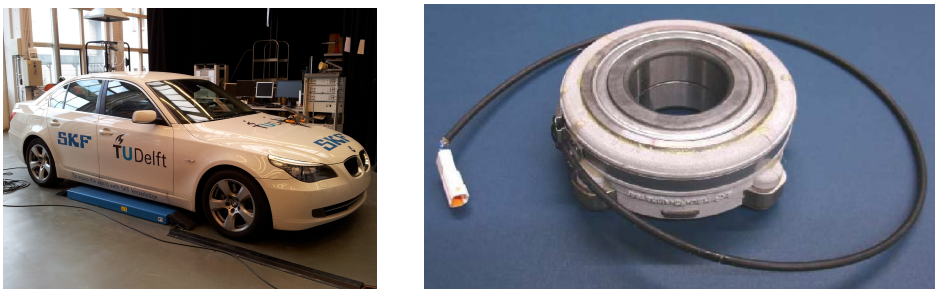

(a) The instrumented test vehicle. (b) The LSB technology from SKF.

Figure 2: The instrumented test vehicle and LSB technology from SKF.

This technology is based on six strain gauges mounted on the bearing. These strains are then processed and transformed into the longitudinal, lateral and vertical components of tyre forces, as explained in [33]. The LSB is an industrially viable solution as it uses strain gauges, a mature technology, whose wholesale price is typically less than 100 US dollar. The wheel bearing is also a mature technology that is affordable and the industrial partner, SKF, is a pioneer in bearing technology.

The LSB is calibrated with the Corrsys sensor using Multiple Linear Regression Analysis (MLRA) between the six LSB strain gauge measurements and the Corrsys sensor measurements [53]. Figures 3-5 show the LSB longitudinal and lateral tyre force measurements of all four test vehicle tires during a J turn, Slalom and Lane Change maneuver.

Table 1 shows the standard deviation (SD) between the LSB and Corrsys measurements from the three maneuvers. In table, SD is the standard deviation of the measurement error of an

Table 1: Standard deviation (SD) between the LSB and Corrsys measurements

Maneuver	Force	SD	SD_{pmt}	SD_{pmvp}	Bias	Bias_{pmt}	Bias_{pmvp}
J turn	F_x	708.48 N	8.0 %	3.0 %	-65.48 N	0.8 %	0.3 %
J turn	F_y	904.41 N	9.5 %	4.5 %	-923.63 N	9.7 %	4.6 %
Slalom	F_x	695.16 N	7.7 %	2.9 %	-38.61 N	0.4 %	0.2 %
Slalom	F_y	678.81 N	7.1 %	3.4 %	103.50 N	1.1 %	0.5 %
Lane Change	F_x	795.57 N	9.0 %	3.4 %	-69.75 N	0.8 %	0.3 %
Lane Change	F_y	752.83 N	7.9 %	3.7 %	-3.42 N	0.04 %	0.02 %

individual tyre force, SD_{pmt} is the standard deviation of the measurement error of an individual

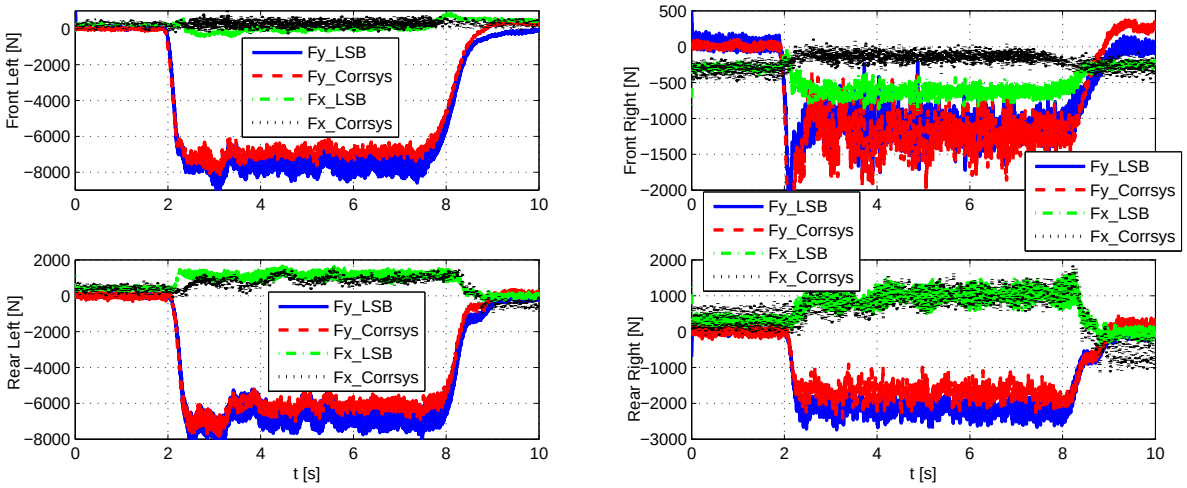

(a) Left tyre forces.

(b) Right tyre forces.

Figure 3: LSB and Corrsys tyre force measurements during a J turn maneuver at an initial speed of 100 km/h.

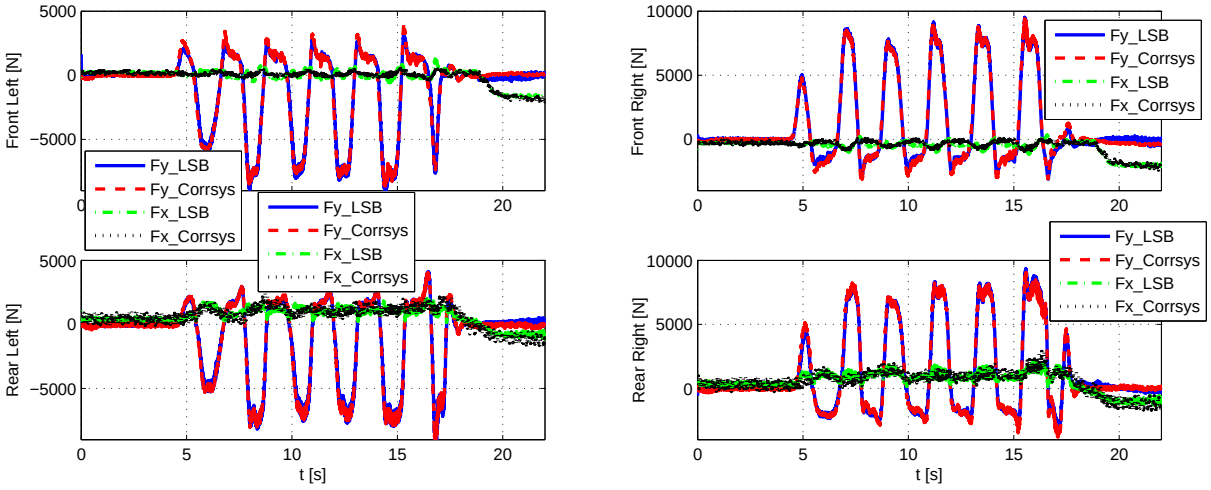

(a) Left tyre forces.

(b) Right tyre forces.

Figure 4: LSB and Corrsys tyre force measurements during a Slalom maneuver at an initial speed of 60 km/h.

tyre force as a percentage of the maximum tyre force, SD_{pmvp} is the standard deviation of the measurement error of the total vehicle planar force as a percentage of the maximum vehicle planar force, Bias is the mean error of an individual tyre force, Bias_{pmt} is the mean error of an individual tyre force as a percentage of the maximum tyre force and Bias_{pmvp} is the mean error of the vehicle planar force as a percentage of the maximum vehicle planar force. In (4), $F_{x_{ij}}$ and $F_{y_{ij}}$ are individual tyre forces of ij tyre, and F_x and F_y are the vehicle planar forces. The vehicle planar forces F_x and F_y are inputs to the vehicle sideslip estimator. Therefore from Table 1, it is seen that using the LSB technology, in the worst case scenario, the estimator inputs F_x and F_y has less than

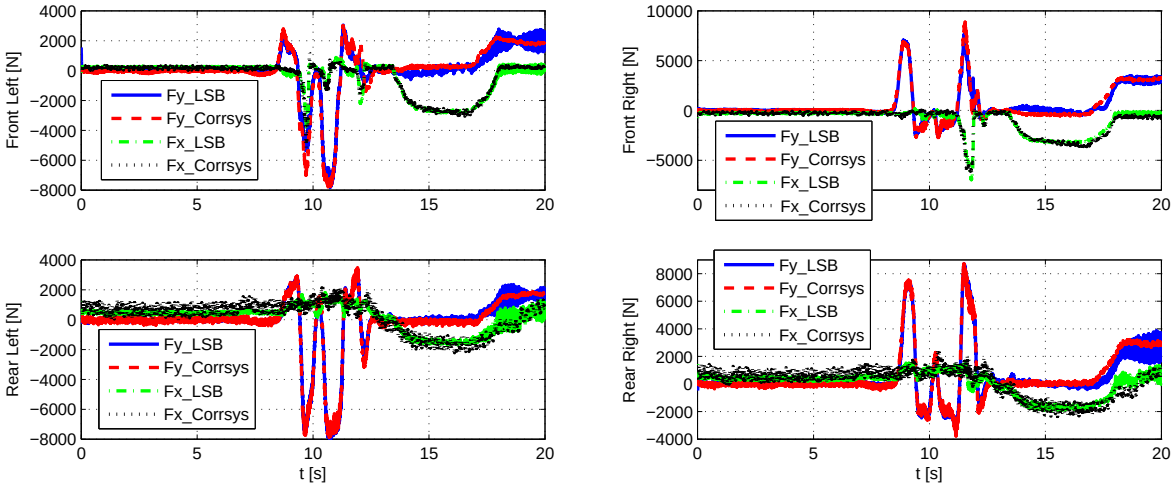

(a) Left tyre forces.

(b) Right tyre forces.

Figure 5: LSB and Corrsys tyre force measurements during a Lane Change maneuver at an initial speed of 104 km/h.

5% standard deviation error and bias as a percentage of their maximum. The LSBs have offsets in the longitudinal and lateral measurements. The longitudinal offset tends to drift with time at a rate of 6.25 N/s approximately and the lateral offset at a rate of 5.17 N/s approximately compared to the Corrsys measurements. They are compensated using the method described in Section 4.3. Overall, LSB's provide an accurate measurement of the tyre forces.

3.1. LSB noise model

The above LSB error analysis summarizes the measurement device performance. In order to derive a more accurate sensor model for the simulation study, the measurement error is studied in the time and frequency domains. Figure 6 plots this analysis for test performed at constant velocity. The measurement noise is not a white noise; but it has two main harmonics. The tire revolution frequency causes the harmonic at 16 Hz whereas the load sensing bearing hub dynamics, specifically the bearing balls, cause the harmonic at 200 Hz. Both harmonics are velocity dependent and are modeled as an additive noise generated by a resonant parameter-varying 4^{th} order linear model fed with a white noise. Figure 6 also plots the validation of the proposed noise model, showing a good match. This noise model is incorporated in all simulations discussed in the paper.

4. Kalman-based vehicle sideslip estimation

In this section, a Kalman filter [38] is designed as the vehicle sideslip estimator. Before the estimator is designed, the system observability is studied.

4.1. Observability Analysis

The observability of the system is studied when the vehicle is going straight. In (8), the observability matrix of the system (5)-(6) results

$$O_{ob} = \begin{bmatrix} C \\ CA(t) \end{bmatrix} = \begin{bmatrix} 1 & 0 \\ 0 & \dot{\psi} \end{bmatrix}. \tag{8}$$

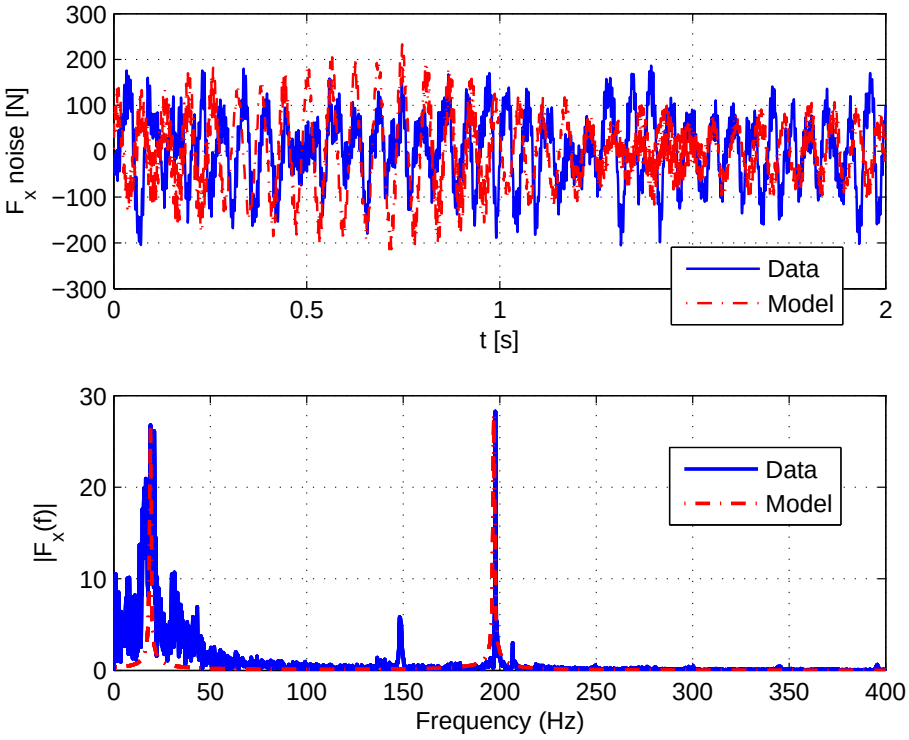

Figure 6: Sample F_x noise data from the test vehicle equipped with load sensing bearings, its frequency spectrum, sample noise model output and the noise model bode plot.

When the vehicle is going straight, the vehicle yaw rate $\dot{\psi}$ is zero and therefore the observability matrix O_{ob} loses full rank. Hence an estimator designed based on the system in (5) and (6) would drift due to unobservability. To handle this unobservability issue, the open loop estimator dynamics in (3) is artificially modified as shown in (9) when $|\dot{\psi}| < 0.1$ deg/s and $|F_y| < 100$ N.

$$\begin{bmatrix} \dot{\hat{v}}_x \\ \dot{\hat{v}}_y \end{bmatrix} = \begin{bmatrix} 0 & \dot{\psi} \\ -\dot{\psi} & f_v \end{bmatrix} \begin{bmatrix} \hat{v}_x \\ \hat{v}_y \end{bmatrix} + \begin{bmatrix} \frac{1}{m} & 0 \\ 0 & \frac{1}{m} \end{bmatrix} \begin{bmatrix} F_x \\ F_y \end{bmatrix}. \tag{9}$$

In the above equation, f_v is a negative valued function as shown in Figure 7 and is defined as:

$$f_v = \begin{cases} -20\left(1 - \frac{\dot{\psi}^2}{\left(0.1\frac{\pi}{180}\right)^2}\right), & \text{if } |\dot{\psi}| < 0.1 \text{ deg/s and } |F_y| < 100 \text{ N} \\ 0, & \text{otherwise} \end{cases} \tag{10}$$

The term f_v is defined as a function of yaw rate to provide a smooth intervention of the observability correction so that the estimate smoothly decays to zero. When $|\dot{\psi}|$ is close to zero and $|F_y| < 100$ N, with the modified estimator dynamics in (9), the lateral velocity estimate $\hat{v}_y$ and therefore the sideslip estimate $\hat{\beta}$ converge to zero as the eigenvalue corresponding to $\hat{v}_y$ becomes negative. This is equivalent to adding an artificial, stabilizing, dynamics to the vehicle when the yaw rate is close to zero. Although this is not physically motivated, it is a reasonable heuristics. In fact, the only

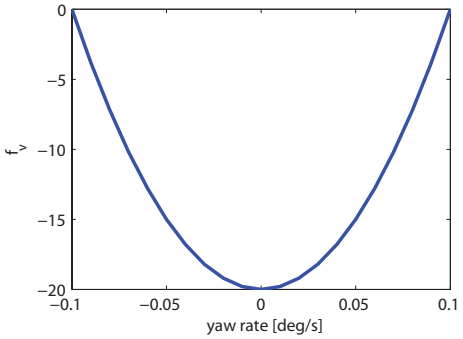

Figure 7: f_v as a function of vehicle yaw rate.

driving scenarios compatible with the low yaw rate and small lateral force conditions are either straight driving with negligible sideslip or pure, stable lateral drift on very low friction surfaces. The latter is a very rare condition that can be discarded. A loss of stability on very low friction is indeed possible, but the vehicle dynamics analysis shows that in those conditions the vehicle would not be stable and thus the yaw rate would not be small. This method to determine whether the vehicle is going straight is similar to the approach used in [41], where if the yaw rate is below a defined threshold for a given period, it is assumed that the vehicle is going straight. However our approach, not being time-triggered and being based on the smooth characteristic defined in (10), yields a smoother estimation dynamics.

4.2. Estimator Design

The estimator is designed using the modified system dynamics in (9). The continuous-time state space model in (5) and (6) with $A(t) = \begin{bmatrix} 0 & \dot{\psi} \\ -\dot{\psi} & f_v \end{bmatrix}$ is discretized as a linear time-varying system:

$$x(k+1) = A(k)x(k) + B(k)u(k) + w(k), \tag{11}$$

$$y(k) = C(k)x(k) + v(k). \tag{12}$$

As shown in Figure 8, the Kalman filter estimates both the present state $\hat{x}(k|k) = \begin{bmatrix} \hat{v}_x(k|k) \\ \hat{v}_y(k|k) \end{bmatrix}$ and the one-step-ahead state $\hat{x}(k+1|k) = \begin{bmatrix} \hat{v}_x(k+1|k) \\ \hat{v}_y(k+1|k) \end{bmatrix}$ of the time varying system. The following equations (13)-(15) describe the present state $\hat{x}(k|k)$ [39].

$$K'(k) = P(k|k-1) \times C(k)^T \left[R + C(k) P(k|k-1) C(k)^T \right]^{-1}, \tag{13}$$

$$\hat{x}(k|k) = \hat{x}(k|k-1) + K'(k) \left[y(k) - C(k) \hat{x}(k|k-1) \right], \tag{14}$$

$$P(k|k) = P(k|k-1) - K'(k) C(k) P(k|k-1), \tag{15}$$

where $K'(k)$ is the Kalman gain, $P(k|k-1)$ is the one-step-ahead state error covariance matrix at time $k-1$, R is the measurement noise covariance matrix, $\hat{x}(k|k)$ is the state estimate at time k, $\hat{x}(k|k-1)$ is the one-step-ahead state estimate at $k-1$ and $P(k|k)$ is the state error covariance

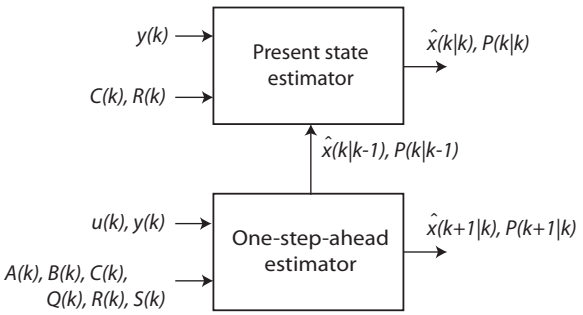

Figure 8: Kalman filter block diagram.

matrix at time k. The following equations (16)-(18) describe the one-step-ahead predicted state $\hat{x}(k+1|k)$:

$$K\left(k\right)=\left[S+A\left(k\right)P\left(k|k-1\right)C\left(k\right)^{T}\right]\left[R+C\left(k\right)P\left(k|k-1\right)C\left(k\right)^{T}\right]^{-1}, \tag{16}$$

$$\hat{x}\left(k+1|k\right)=A\left(k\right)\hat{x}\left(k|k-1\right)+B\left(k\right)u\left(k\right)+K\left(k\right)\left[y\left(k\right)-C\left(k\right)\hat{x}\left(k|k-1\right)\right], \tag{17}$$

$$P\left(k+1|k\right)=A\left(k\right)P\left(k|k-1\right)A\left(k\right)^{T}+Q-K\left(k\right)\left[S+A\left(k\right)P\left(k|k-1\right)C\left(k\right)^{T}\right]^{T}, \tag{18}$$

where $K(k)$ is the Kalman gain, S is the cross-correlation matrix between the process and measurement noise, $\hat{x}(k+1|k)$ is the one-step-ahead state estimate at time k, $P(k+1|k)$ is the one-step-ahead state error covariance matrix at time k and Q is the process noise covariance matrix.

For the simulation studies, the measurement noise covariance R is calculated from a sample output measurement noise from the test vehicle. The process noise covariance Q is tuned during the estimator implementation and the cross-correlation S is assumed to be zero. For studies with the test data, Q and R matrices are found using an optimization algorithm. This is further discussed in Section 6.2.

From the present state estimate $\hat{x}(k|k)=\begin{bmatrix}\hat{v}_x(k|k)\\ \hat{v}_y(k|k)\end{bmatrix}$, the vehicle sideslip estimate $\hat{\beta}(k)$ is calculated as:

$$\hat{\beta}(k)=\frac{\hat{v}_y(k|k)}{\hat{v}_x(k|k)}. \tag{19}$$

4.3. Sensor offset compensation

Vehicle sideslip estimators are sensitive to sensor offset values. For example, the effects of longitudinal and lateral accelerometer offsets are studied and reported in [37]. The analysis of the sensor bearings performance has shown that also LSB's have offsets in the longitudinal and lateral measurements. The following algorithm is used to compensate for them.

$$\begin{aligned} IF\ |T_{EN}|<2\ \text{Nm}\ AND\ P<0.1\ \text{bar}\\ F_x^{offset}=\text{moving average}(F_x)\end{aligned} \tag{20}$$

$$\begin{aligned} IF\ |\delta|<0.1\ \text{deg}\ AND\ |\dot{\psi}|<0.01\ \text{deg/s}\\ F_y^{offset}=\text{moving average}(F_y)\end{aligned} \tag{21}$$

The moving average is calculated over a period of 0.2 s. In this duration, 100 measurement samples are available. Here T_{EN} is the engine torque and P is the brake pressure. The pressure is often directly measured, while an estimation of the engine torque is available on all modern engines. Note that the offset bias compensation method presented in [37] could be applied to the force sensors as well.

5. Accelerometer based vehicle sideslip estimator

In this section, the accelerometer based vehicle sideslip estimator used to benchmark the proposed estimator is introduced. The accelerometer based sideslip estimator is an implementation of the Kinematic model-based observer design proposed in [18]. The process noise covariance Q and measurement noise covariance R are tuned according to the same approach used to tune the force based estimator. The cross-correlation S is assumed to be zero.

6. Results

In this section, two sets of studies are performed and their results discussed:

1. First, various simulation tests are conducted with different configurations of the proposed vehicle sideslip estimator. The vehicle model being simulated is the CarSim multi-body model explained in Section 1.
2. Next, the proposed estimator is validated with test data from a BMW 5 Series E60 test vehicle. Here the objective is to study the effectiveness of the estimator in a real vehicle. This is further discussed in Section 6.2.

6.1. Simulation Studies

In the following simulation studies, n order to account for the LSB noise in these simulations, the longitudinal and lateral tyre force measurements from CarSim are polluted with filtered white noise according to the noise model identified in Section 3.1.

In the first simulation, the estimator is studied with the Sine with Dwell (SWD) steering input shown in Figure 9 at a speed of 80 km/h. In this simulation, no measurement bias is considered. From the results shown in Figure 9, it is observed that the accelerometer based estimate does not track the reference well. This is caused by the roll and pitch dynamics, whereas the force based estimator is accurate. Due to the roll and pitch angle, the accelerometer measurements are not same as the accelerations on the road plane and this error affects the accuracy of the accelerometer based estimator. The differences in accelerations and the roll and pitch angle causing them are shown in Figure 10. Although the differences in accelerations in Figure 10 look small in magnitude, the sideslip estimator is sensitive to these differences because of its integral nature. On the other hand, as the measured tyre forces represent the forces acting at the road-tyre contacts, the force based estimate is not corrupted by the roll and pitch dynamics. It should be noted that even though the roll angle converges to zero for $t > 2.5$ s, the accelerometer based estimate does not converge to zero for $t > 2.5$ s because of the unobservability issue previously discussed. For the considered SWD maneuver, in the lateral acceleration range $\{-0.9, 0.9\}$ g, the force based estimator is able to estimate vehicle sideslip with RMSE less than 0.1° and Normalized RMSE (NRMSE) less than 2% as shown in Table 2.

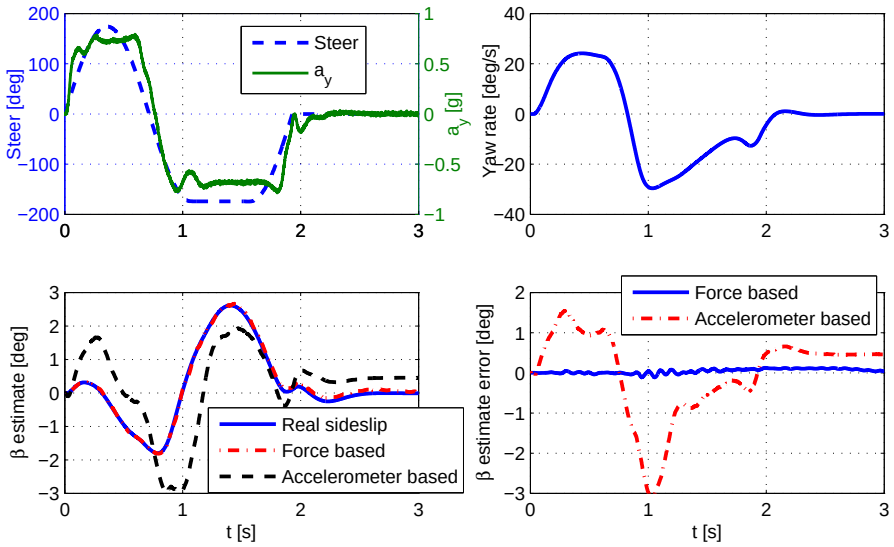

Figure 9: Vehicle sideslip estimation during the Sine with Dwell maneuver at a vehicle speed of 80 km/h.

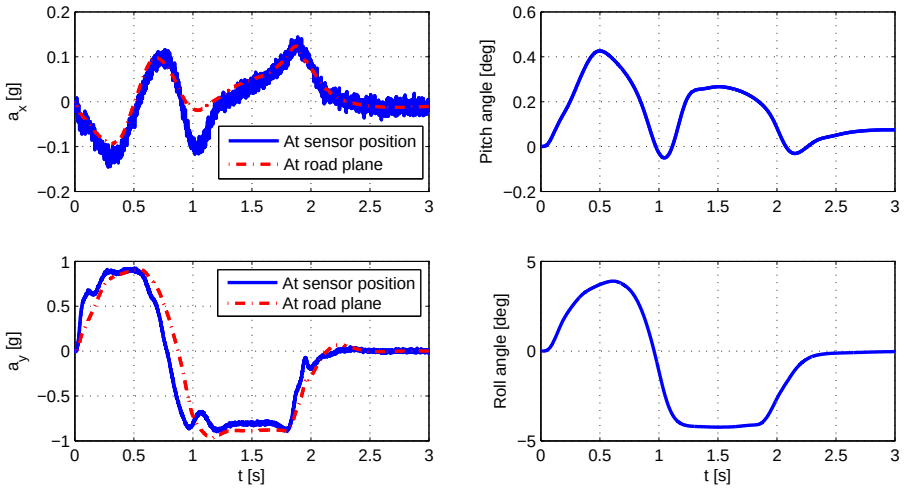

Figure 10: Vehicle accelerations, roll angle and pitch angle during the Sine with Dwell maneuver at 80 km/h.

Table 2: Estimator Root Mean Square Error

Simulation type	$RMSE_{force}$	$RMSE_{acc}$	$NRMSE_{force}$	$NRMSE_{acc}$
Sine with Dwell	0.0716°	1.0662°	1.62%	24.14%
Double Lane Change	0.0481°	0.8282°	1.07%	24.52%
Fish Hook	0.1342°	1.3517°	4.57%	46.47%
Low friction	0.7205°	6.0218°	3.05%	25.47%

Figures 11-13 plot the results for the Double Lane Change, Fish Hook and low friction maneuvers. The RMSE values of these simulations are shown in Table 2. The Double Lane Change and Fish Hook maneuver simulation results in Figure 11 and 12 show that the force measurement based estimator yields better accuracy than the accelerometer based estimator. As mentioned before, the unmodeled roll and pitch dynamics degrade the accelerometer based estimator accuracy. From Table 2, the force measurement based estimator estimates the sideslip with RMSE less than 0.15° and NRMSE less than 5 %.

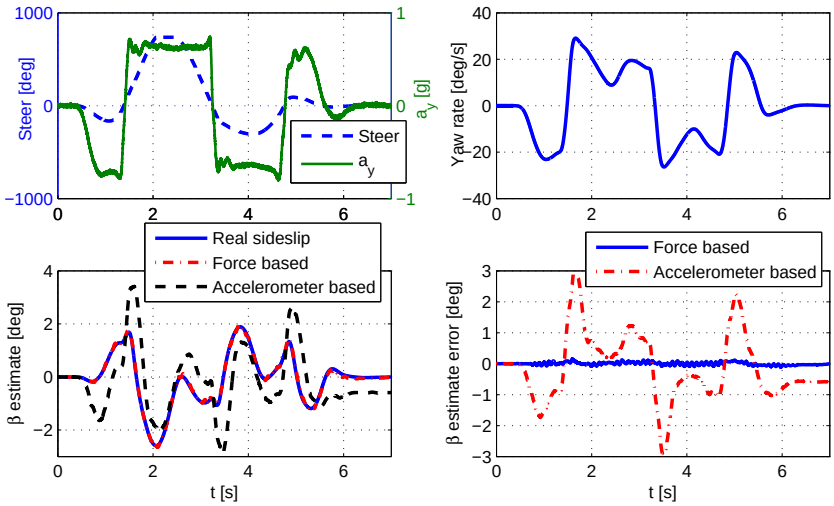

Figure 11: Vehicle sideslip estimation during the Double Lane Change maneuver with a vehicle speed of 80 km/h.

Next, the approach is tested on a low friction surface with friction 0.2. Figure 13 plots the throttle and steering wheel inputs. They are chosen such that the vehicle experiences combined slip with high vehicle sideslip values. Figure 13 and Table 2 show that even on low friction surfaces, the force measurement based estimator estimates the vehicle sideslip accurately. This is an advantage with respect to the physical model-based estimators discussed in Section 1 that need information on the friction characteristics. Table 2 lists a 6° RMSE for the accelerometer based estimator, whereas the force based estimator gives a RMSE of less than 0.8°. Furthermore, in general the estimation errors on low friction are larger; this effect is due the higher sideslip angles reached on low friction surfaces. When normalized, the estimation errors are comparable.

The unobservability issue is studied in detail with a SWD maneuver at a vehicle speed of 80 km/h in the presence of an artifical 200 N measurement bias in F_y. The SWD steering profile as well as the simulation results are shown in Figure 14. It is seen that without the unobservability correction, the estimate is not accurate. The unobservability issue causes the estimate to drift, whereas with the unobservability correction discussed in Section 4.1, the vehicle sideslip estimate is accurate throughout the maneuver. This is seen in Figure 14. The unobservability issue is also seen in the low friction simulation results of Figure 13. As the accelerometer based estimator does not have the unobservability correction, when $t > 22$ s, the vehicle sideslip estimate drifts to higher negative values. It is indeed important for VDC systems to have an accurate sideslip estimate in such low friction situations because they are critical from a vehicle stability point of view. With the unobservability correction, the force measurement based estimate is accurate and there is no

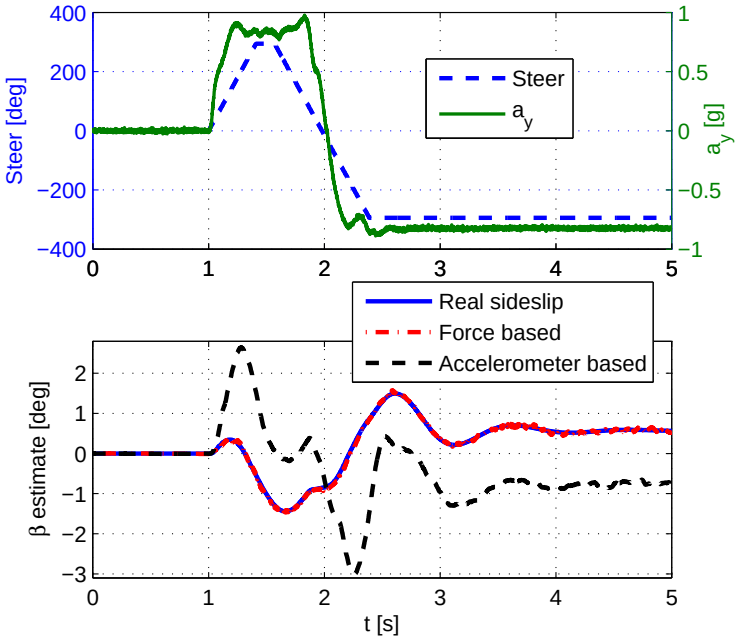

Figure 12: Vehicle sideslip estimation during the Fish Hook maneuver with a vehicle speed of 79 km/h.

drift when $t > 22$ s.

6.2. Validation with Experimental Data

Here, the proposed vehicle sideslip estimator is validated using experimental data acquired with the test vehicle. A BMW 5 Series E60 model is used as the test vehicle. The force based estimator is also compared with the accelerometer based estimator. The test vehicle is equipped with LSB on all four tires. The vehicle is also equipped with front road wheel steer angle sensors, wheel angular velocity sensors, accelerometers in longitudinal and lateral directions, yaw rate sensor and laser speed sensors in longitudinal and lateral directions. The test data is collected at the ATP proving ground in Papenburg, Germany. The estimation algorithms do not employ the information from the optical sensor. The optical speed sensor is only employed to compute the real sideslip against which the algorithm are compared.

The force measurement based vehicle sideslip estimator is validated with test data from J turn, Lane Change and Slalom maneuvers. The Q and R matrices are initialized with their values from the simulation studies, and are further tuned using a constrained optimization algorithm. The optimization objective is to minimize the integral of the absolute value of the estimation error in the considered three maneuvers and it is a constrained optimization such that $Q > 0$ and $R > 0$. The same procedure is used to tune the accelerometer based estimator. For the force based estimator, the optimized values of Q and R are $\begin{bmatrix} 0.1805 & 0 \\ 0 & 1.0167 \end{bmatrix}$ and 0.001 respectively, and for the accelerometer based estimator, the optimized values of Q and R are $\begin{bmatrix} 0.1 & 0 \\ 0 & 1.0 \end{bmatrix}$ and 0.01 respectively. Note that this procedure yields a single tuning for each method. The tuning is not

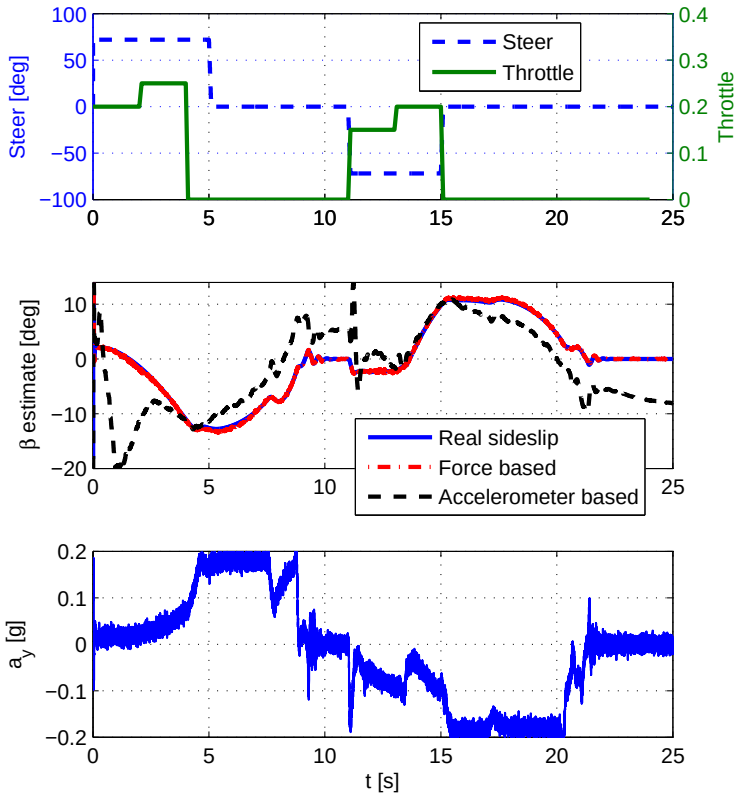

Figure 13: Vehicle sideslip estimation with road friction 0.2.

changed among different maneuvers.

The J turn maneuver is performed at an initial vehicle speed of 100 km/h; Figure 15 plots the steering profile. From Figure 15, it is observed that both the LSB based and accelerometer based estimators are accurate during the maneuver. However, the accelerometer based estimate drifts for $t > 9$ s due to the unobservability, whereas the LSB based estimate is accurate for $t > 9$ s. Figure 3 shows the longitudinal and lateral force measurements of all four tires.

Further validation of the estimator is performed with the experimental data from the Slalom and Lane Change maneuvers. The results are shown in Figures 16 and 17. The vehicle experiences lateral acceleration in the range $\{-1, 1\}$ g as seen in the plots. In both maneuvers, the LSB based method estimates the vehicle sideslip accurately and gives better estimates compared to the accelerometer based approach. In addition, the accelerometer based estimates drift when the vehicle is going straight because of the unobservability issue, whereas the LSB based estimates do not drift as the issue is addressed as discussed in Section 4.1.

An interesting event happens during the Lane Change maneuver around $t = 11.75$ s. The accelerometer based estimate has high error. This happens because the Lane Change maneuver is pushing the vehicle to its limits. This is evident from the top plot of Figure 5(b) as ESC intervention (severe braking only on the front right tyre) is present around $t = 11.75$ s. During

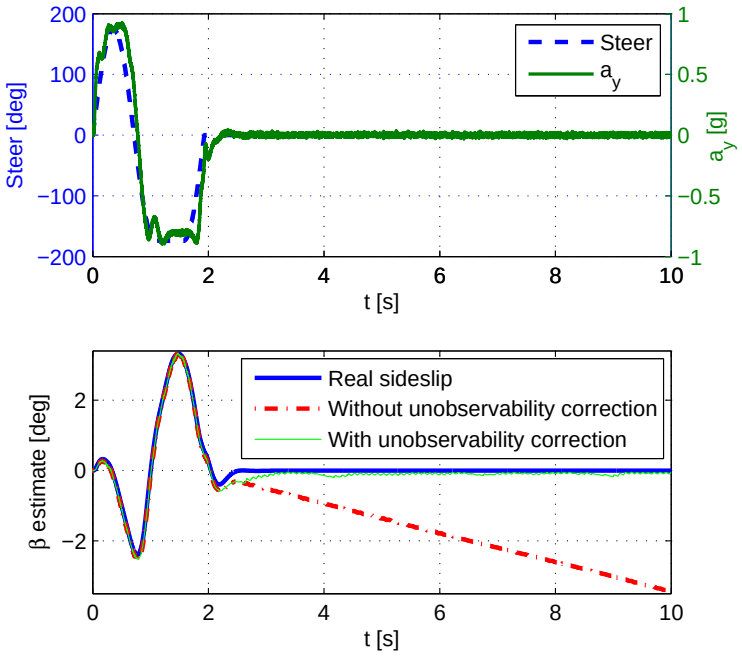

Figure 14: Vehicle sideslip estimation during Sine with Dwell maneuver at 80 km/h in the presence of 200 N measurement bias in F_y demonstrating the unobservability issue when the yaw rate is close to zero.

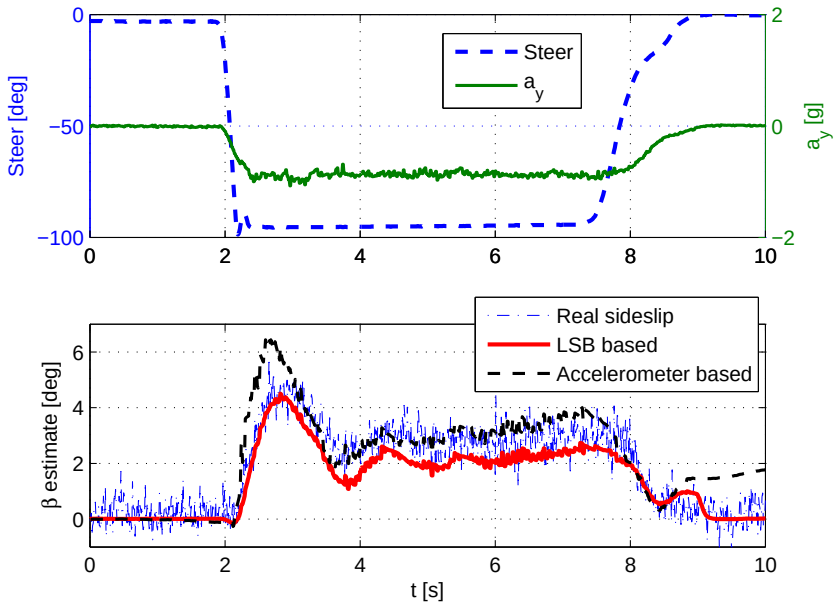

Figure 15: Vehicle sideslip estimation using test data from a J turn maneuver at an initial vehicle speed of 100 km/h.

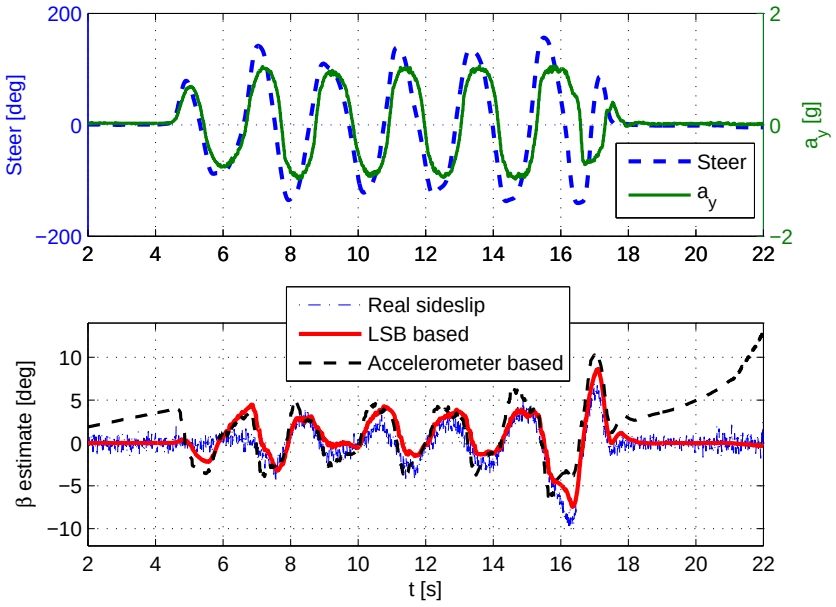

Figure 16: Vehicle sideslip estimation using test data from a Slalom maneuver at an initial vehicle speed of 60 km/h.

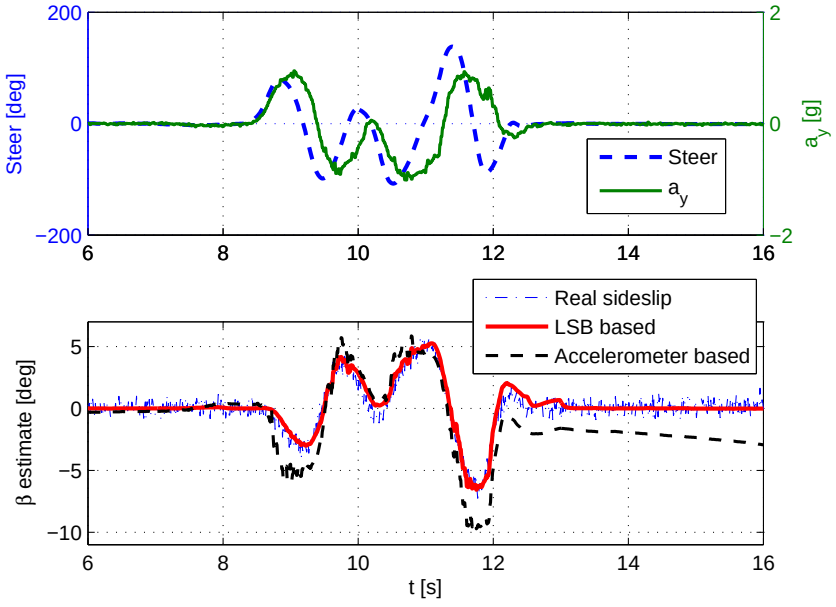

Figure 17: Vehicle sideslip estimation using test data from Lane Change maneuver at an initial vehicle speed of 104 km/h.

this time, pitch and roll dynamics are present, and the accelerometer based estimator is no more accurate, whereas the LSB based estimator maintains its performance. A similar event happens at around $t = 9$ s and is caused by another ESC intervention (as apparent from the braking of only

the front left tyre in Figure 5(a)). These events demonstrate that the proposed LSB based vehicle sideslip estimator is accurate during critical maneuvers. From the validation results in Figures 15, 16 and 17, it is concluded that the LSB based vehicle sideslip estimator is suitable for sideslip estimation in a real vehicle.

7. Conclusions

A Load Sensing Bearing based vehicle sideslip estimator is proposed in this work. Using the vehicle kinematic model, a Kalman filter is designed and studied as the vehicle sideslip estimator. This work also proposes a heuristic method to handle the unobservability issue with the kinematic model-based vehicle sideslip estimation while the yaw rate is close to zero. The proposed estimator is extensively validated on a BMW 5 Series E60 model test vehicle equipped with LSB technology.

The proposed vehicle sideslip estimator is tested using simulation studies as well as test data. From the simulation studies with Sine with Dwell, Double Lane Change, Fish Hook and low friction manuevers, the proposed estimator is found to be accurate with RMSE values shown in Table 2. Compared to the accelerometer based vehicle sideslip estimator, the proposed force based estimator is found to be more accurate. The benefit is mainly due to the insensitivity of the force based method to the roll and pitch dynamics. In the lateral acceleration range $\{-0.9, 0.9\}$ g, the proposed estimator shows good accuracy.

The vehicle sideslip estimator is also validated with experimental data from the test vehicle during a J turn, Lane Change and Slalom maneuver. The results show good accuracy in the sideslip estimation when compared with the real sideslip calculated using the laser speed sensors equipped in the test vehicle, and the estimator is more accurate than the accelerometer based vehicle sideslip estimator. The proposed estimator is also observed to be accurate during ESC interventions. The ongoing research focuses on more accurate methods to calculate tyre force measurements from the LSB strain gauges and to remove the LSB offsets.

Acknowledgements

We would like to thank Sven Jansen, Sr. Scientific Research Engineer, Netherlands Organization for Applied Scientific Research (TNO), Helmond, The Netherlands and Henk Mol, Scientist, SKF Engineering and Research Center, Nieuwegein, The Netherlands for their prompt email discussions and support.

References

References

[1] K. Reif, "Bosch Professional Automotive Information: Fundamentals of Automotive and Engine Technology," Springer Fachmedien Wiesbaden, 2014.

[2] A. Hoye, "The effects of Electronic Stability Control (ESC) on crashes an update," Accident Analysis & Prevention, vol. 43, no. 3, pp. 1148-1159, May 2011.

[3] M. Abe, Y. Kano, K. Suzuki, Y. Shibahata and Y. Furukawa, "Side-slip control to stabilize vehicle lateral motion by direct yaw moment," *Society of Automotive Engineers of Japan Review*, vol. 22, no. 4, pp. 413-419, October 2001.

[4] R. Tchamna and I. Youn, "Yaw rate and side-slip control considering vehicle longitudinal dynamics," *International Journal of Automotive Technology*, vol. 14, no. 1, pp. 53-60, February 2013.

[5] Y. Shibahata, K. Shimada and T. Tomari, "Improvement of Vehicle Maneuverability by Direct Yaw Moment Control," *Vehicle System Dynamics: International Journal of Vehicle Mechanics and Mobility*, vol. 22, no. 5-6, pp. 465-481, 1993.

[6] Van Zanten and Anton T. "Evolution of electronic control systems for improving the vehicle dynamic behavior," *Proceedings of the 6th International Symposium on Advanced Vehicle Control*, 2002.

[7] Van Zanten, Anton T., R. Erhardt and G. Pfaff, "VDC, the vehicle dynamics control system of Bosch," *SAE Technical Paper*, no. 950759, 1995.

[8] S. Inagaki, I. Kshiro and M. Yamamoto, "Analysis on vehicle stability in critical cornering using phase-plane method," *Proceedings of the International Symposium on Advanced Vehicle Control*, Tsukuba-shi, Japan, 1994.

[9] J. Ryu, E. J. Rossetter and J. C. Gerdes, "Vehicle sideslip and roll parameter estimation using GPS," *In Proceedings of the AVEC International Symposium on Advanced Vehicle Control*, 2002.

[10] J. Stephant, A. Charara and D. Meizel, "Virtual sensor: application to vehicle sideslip angle and transversal forces," *IEEE Transactions on Industrial Electronics*, vol. 51, no. 2, pp. 278,289, April 2004.

[11] J. Stephant, A. Charara and D. Meizel, "Evaluation of a sliding mode observer for vehicle sideslip angle," *Control Engineering Practice*, vol. 15, no. 7, pp. 803-812, July 2007.

[12] H. B. Pacejka and E. Bakker, "THE MAGIC FORMULA TYRE MODEL," *Vehicle System Dynamics*, vol. 21, supplement 1, pp. 1-18, 1992.

[13] G. Gim and P. E. Nikravesh, "An analytical model of pneumatic tyres for vehicle dynamic simulations. Part 1: pure slips," *International Journal of Vehicle Design*, vol. 11, no. 6, pp. 589-618, 1990.

[14] Y. Zhang and J. Yi, "Static Tire/Road Stick−Slip Interactions: Analysis and Experiments," *IEEE/ASME Transactions on Mechatronics*, vo. 19, no. 6, pp. 1940-1950, 2014.

[15] G. Baffet, A. Charara and D. Lechner, "Estimation of vehicle sideslip, tire force and wheel cornering stiffness," *Control Engineering Practice*, vol. 17, no. 11, pp. 1255-1264, November 2009.

[16] Seung-Han You, Jin-Oh Hahn and H. Lee, "New adaptive approaches to real-time estimation of vehicle sideslip angle," *Control Engineering Practice*, vol. 17, no. 12, pp. 1367-1379, December 2009.

[17] G. Phanomchoeng, R. Rajamani, and D. Piyabongkarn, "Nonlinear observer for bounded Jacobian systems, with applications to automotive slip angle estimation" *IEEE Transactions on Automatic Control*, vol. 56, no. 5, pp. 1163-1170, 2011.

[18] J. Farrelly, P. Wellstead, "Estimation of vehicle lateral velocity," *Proceedings of the 1996 IEEE International Conference on Control Applications*, pp. 552-557, September 1996.

[19] J. Oh, Y. Noh and S. B. Choi, "Real-time offset error compensation of 6D IMU mounted on ground vehicles using disturbance observer," *Proceedings of the International Conference on Intelligent Information and Networks*, Male, Maldives, February 2013.

[20] D. Piyabongkarn, R. Rajamani, J. A. Grogg and J. Y. Lew, "Development and experimental evaluation of a slip angle estimator for vehicle stability control," *IEEE Transactions on Control Systems Technology*, vol. 17, no. 1, pp. 78-88, 2009.

[21] M. Corno, M. Gerard, M. Verhaegen and E. Holweg, "Hybrid ABS Control Using Force Measurement," *IEEE Transactions on Control Systems Technology*, vol. 20, no. 5, pp. 1223-1235, September 2012.

[22] Y. Zhang, J. Yi and T. Liu, "Embedded Flexible Force Sensor for In-Situ Tire-Road Interaction Measurements," *IEEE Sensors Journal*, vol. 13, no. 5, pp. 1756-1765, May 2013.

[23] K. Nam, H. Fujimoto and Y. Hori, "Motion control of electric vehicles based on robust lateral tire force control using lateral tire force sensors," *2012 IEEE/ASME International Conference on Advanced Intelligent Mechatronics (AIM)*, pp. 526-531, 11-14 July 2012.

[24] K. Nam, H. Fujimoto and Y. Hori, "Advanced motion control of electric vehicles based on robust lateral tire force control via active front steering," *IEEE/ASME Transactions on Mechatronics*, vol. 19, no. 1, pp. 289-299, 2014.

[25] D. Gunji and H. Fujimoto, "Measurement Performance Evaluation of Lateral Tire Force Sensor for Yaw-rate Control of Electric Vehicle," *EVTeC and APE Japan 2014, Society of Automotive Engineers of Japan*, 2014.

[26] G. Lin, H. Pang, W. Zhang, D. Wang, and L. Feng, "A self-decoupled three-axis force sensor for measuring the wheel force," *Proceedings of the Institution of Mechanical Engineers, Part D: Journal of Automobile Engineering*, 2013.

[27] M. Gerard, M. Corno, Michel Verhaegen, E. Holweg, "Force-Based ABS Control Using Lateral Force Measurement," *ASME 2011 Dynamic Systems and Control Conference and Bath/ASME Symposium on Fluid Power and Motion Control (DSCC2011)*, Arlington, Virginia, USA, vol. 2, pp. 831-837, 2011.

[28] E. de Bruijn, M. Gerard, M. Corno M. Verhaegen and E. Holweg, "On the performance increase of wheel deceleration control through force sensing," *IEEE International Conference on Control Applications*, Yokohama,

Japan, pp. 161-166. Sept. 2010.
[29] A. K. Madhusudhanan, M. Corno and E. Holweg, "Lateral Vehicle Dynamics Control Based On Tyre Utilization Coefficients and Tyre Force Measurements," 52^{nd} *IEEE Conference on Decision and Control*, Florence, Italy, pp. 2816-2821, 10-13 December 2013.
[30] A. K. Madhusudhanan, M. Corno and E. Holweg, "Sliding Mode Based Lateral Vehicle Dynamics Control Using Tyre Force Measurements," *Submitted to Vehicle System Dynamics: International Journal of Vehicle Mechanics and Mobility*, February 2015.
[31] A. K. Madhusudhanan, M. Corno and E. Holweg, "Vehicle Sideslip Estimation Using Tyre Force Measurements," *submitted to the 23rd Mediterranean Conference on Control & Automation*, Torremolinos, Spain, June 16-19, 2015.
[32] "CarSim Math Models," *Mechanical Simulation Corporation Brochures & Tech Memos*, September 2012.
[33] B. G. Van Leeuwen, E. G. M. Holweg, F. Wit, E. Zaaijer and S. Ballegooij, "Measurement device for measuring radial and/or axial forces," *U.S. Patent No. 6,920,801.* July 2005.
[34] "Vehicle Dynamics & Durability," *Kistler Brochures*, www.kistler.com.
[35] U. Kiencke and L. Nielsen, "Automotive Control Systems. For Engine, Driveline, and Vehicle," *Springer-Verlag Berlin Heidelberg*, 2005.
[36] S. M. Savaresi and M. Tanelli, "Active Braking Control Systems Design for Vehicles," *Springer London*, 2010.
[37] G. Panzani, M. Corno, M. Tanelli, S. M. Savaresi, A. Fortina and S. Campo, "Control-oriented vehicle attitude estimation with online sensors bias compensation," *ASME 2009 Dynamic Systems and Control Conference*, Hollywood, USA, pp. 819-826, January 2009.
[38] R. E. Kalman, "A new approach to linear filtering and prediction problems," *Transactions of the ASME-Journal of Fluids Engineering*, vol. 82, Series D, pp. 35-45, 1960.
[39] M. Verhaegen and V. Verdult (2007), *Filtering and System Identification: A Least Squares Approach*, Cambridge University Press, New York.
[40] D. M. Bevly, J. Ryu and J. C. Gerdes, "Integrating INS sensors with GPS measurements for continuous estimation of vehicle sideslip, roll, and tire cornering stiffness," *IEEE Transactions on Intelligent Transportation Systems*, vol. 7, no. 4, pp. 483-493, 2006.
[41] J. G. Ryan and D. M. Bevly "On the Observability of Loosely Coupled Global Positioning System/Inertial Navigation System Integrations With Five Degree of Freedom and Four Degree of Freedom Inertial Measurement Units," *Journal of Dynamic Systems, Measurement, and Control*, vol. 136 no. 2, 021023, March 2014.
[42] G. Panzani, M. Corno, M. Tanelli, A. Zappavigna, S. M. Savaresi, A. Fortina and S. Campo, "Designing On-Demand Four-Wheel-Drive Vehicles via Active Control of the Central Transfer Case," *IEEE Transactions on Intelligent Transportation Systems*, vol. 11, no. 4, pp. 931-941, 2010.
[43] M. Corno, M. Tanelli, I. Boniolo and S. M. Savaresi, "Advanced Yaw Control of Four-wheeled Vehicles via Rear Active Differential Braking," *Proceedings of the 48th IEEE Conference on Decision and Control 2009*, pp. 5176-5181, 15-18 December, 2009.
[44] D. M. Bevly, J. C. Gerdes and C. Wilson, "The use of gps based velocity measurements for measurement of sideslip and wheel slip," *Vehicle System Dynamics*, vol. 38, no. 2, pp. 127-147, 2002.
[45] D. M. Bevly, J. Ryu and J. C. Gerdes, "Integrating ins sensors with gps measurements for continuous estimation of vehicle sideslip, roll, and tire cornering stiffness," *IEEE Transactions on Intelligent Transportation Systems*, vol. 7, no. 4, pp. 483-493, 2006.
[46] K. Nam, H. Fujimoto and Y. Hori, "Lateral Stability Control of In-Wheel-Motor-Driven Electric Vehicles Based on Sideslip Angle Estimation Using Lateral Tire Force Sensors," *IEEE Transactions on Vehicular Technology*, vol. 61, no. 5, pp. 1972-1985, Jun 2012.
[47] Yoon, Jong-Hwa and Huei Peng, "Sideslip angle estimation based on GPS and magnetometer measurements," *Proceeding of 11th International Symposium on Advanced Vehicle Control*, 2012.
[48] Yih, Paul, Jihan Ryu and J. Christian Gerdes, "Vehicle state estimation using steering torque," *Proceedings of the 2004 American Control Conference*, 2004.
[49] H. Kim and J. Ryu, "Sideslip angle estimation considering short-duration longitudinal velocity variation," *International Journal of Automotive Technology*, vol. 12, no. 4, pp. 545-553, 2011.
[50] L. Wei, L. Wenying, D. Haitao and G. Konghui, "Side-slip angle estimation for vehicle electronic stability control based on sliding mode observer," *in International Conference on Measurement, Information and Control (MIC) 2012*, pp. 992-995, 2012.
[51] J. J. Oh and S. B. Choi, "Vehicle velocity observer design using 6-d imu and multiple-observer approach," *IEEE Transactions on Intelligent Transportation Systems*, vol. 13, no. 4, pp. 1865-1879, 2012.
[52] D. Piyabongkarn, R. Rajamani, J. A. Grogg and J. Y. Lew, "Development and experimental evaluation of a

slip angle estimator for vehicle stability control," *IEEE Transactions on Control Systems Technology*, vol. 17, no. 1, pp. 78-88, 2009.

[53] J. J. Van Doornik, "Haptic feedback on the steering wheel near the vehicles handling limits using wheel load sensing," *Master thesis, Delft University of Technology, the Netherlands,* 2014.

[54] K. Nam, S. Oh, H. Fujimoto and Y. Hori, "Estimation of Sideslip and Roll Angles of Electric Vehicles Using Lateral Tire Force Sensors Through RLS and Kalman Filter Approaches," *IEEE Transactions on Industrial Electronics*, vol. 60, no. 3, pp. 988-1000, March 2013.